Numerical investigations on passive control of vibration induced by bolted-joint rotor suspended by AMBs

Yang ZHOU*, Jin ZHOU*, Yuanping XU*, Yue ZHANG* and Jarir MAHFOUD**
*College of Mechanical & Electrical Engineering, Nanjing University of Aeronautics and Astronautics
No. 29, Yudao Street, Nanjing, Jiangsu 210016, China
E-mail: zhj@nuaa.edu.cn
**INSA-Lyon, CNRS UMR5259, LaMCoS
INSA-Lyon, F-69621 Villeurbanne Cedex, France

Abstract
Rotor-Active magnetic bearing (rotor-AMB) systems offer significant advantages in power consumption and are increasingly being applied in turbomachinery. However, in such machinery, the impeller and the rotor are commonly connected by bolted-joint. We observed once a certain pre-tightening torque is applied to the bolted connection and the interface contact between the rotor and the impeller is formed, the bending mode vibration will be excited when the rotor is levitated. The conventional active control method is limited in this vibration suppression and it is essential to increase the damping at bending mode to inhibit vibration. This research presents a novel passive control method to suppress this vibration by using the eddy current damping. Numerical simulations were carried out based on the rotor-AMBs system model considering bolted-joint interface contact model and analytical eddy-current damping model. Results obtained show that when decreasing the axial clearance between permanent magnet and the impeller, the eddy-current damping is increased exponentially, which will lead to the suppression of the bending mode response and reduce the vibration amplitude by 99.5%.

Keywords : Active Magnetic Bearing, Bolted-joint Assembly, Eddy Current Damping, Interface Contact, Vibration Suppression

1. Introduction

Active magnetic bearings (AMBs) have been widely used in centrifugal gas compressors and other turbomachinery applications (Schweitzer and Maslen, 2009). In these rotating machineries, several methods could be used to assemble the different components and particularly bolted-joint. As an integrated part of some rotating machinery, an impeller is often assembled by bolted joint in AMB suspended rotating machinery. The bolted-joint could generally be characterized by its torque and its contact radius as shown in Fig. 1. We noticed that (Zhou et al., 2023), when the bolted-joint torque is relatively small (there is contact pressure), a possible relative displacement is induced by the AMB levitating forces, that could lead to the excitation of the structure and could introduce instability for modes that are on the limit of stability. In our previous research (Zhou et al., 2024a), the vibration amplitude increases as the increase of bolted-joint torque and contact radius, the cause of this vibration is the coupling between the bolted-joint interface contact and the AMB levitating forces. The motivation of this paper is to reduce the influence of this vibration. Active control and passive control methods have been proposed.

Based on the active-control characteristic, the active control methods can be divided into two ways: the gain compensation and phase compensation (Schweitzer and Maslen, 2009). Firstly, gain compensation is a type of filter designed to attenuate specific frequencies while allowing others to pass through, typically achieved by creating a resonant circuit that cancels out unwanted frequency components. Han et al. (2021) designed the gain compensation and successively suppressed the bending mode vibration caused by the bolted-joint, which was validated experimentally. However, this gain compensation cannot be applied to the rotor with significant gyroscopic effect since the vibration frequency would be varied greatly and nonlinearly as the increase of rotation speed. Aiming at this challenge, Zeng et al. (2025) optimized the previous gain compensation and the center frequency of gain compensation was able to adjust according to the rotation speed adaptively, which was based on the relationship between vibration frequency and rotation

speed obtained by numerical simulation. However, the simulation is not accurate enough, which will lead to the failure of control. Secondly, phase compensation adjusts the phase of a signal to correct timing differences, improving system stability or response characteristics. Wei et al. (2023) designed the phase compensation and adjusted its parameters to reduce the vibration caused by bolted-joint interface contact in the magnetic suspended turbo molecular pump, but the calculation of the phase needed is not given. To solve this difficulty, Zhou et al. (2024b) introduced the optimal phase calculation method and suppressed the bending mode vibration caused by the bolted-joint, which was validated experimentally. However, the operating range of the phase compensation was limited, which will increase high-frequency gain of closed-loop and excite other unstable modes.

Since active method has limitations in the robustness, some passive methods have been designed to control this vibration. In previous study, the contact stiffness at the interface was reduced by decreasing the preload torque and contact radius. However, the adjusted preload torque and contact radius were too small to meet the assembly requirements for bolted-joint connections in rotating machinery (Zhou et al., 2024a). Only changing the bolted-joint parameters was not enough to suppress this vibration, extra damping should be introduced to the closed-loop system to improve stability. Besides the internal damping provide by the controller (such as phase compensation), the external non-contact damping such as eddy current damping, acoustic damping and piezoelectric damping were also effective in vibration reduction. Considering the space occupancy and sensitivity to material of acoustic damping and piezoelectric damping (Zhu et al., 2024, Park et al., 2011), We noticed that the eddy current damping is more suitable to passive vibration control in the rotor-AMBs system.

In the magnetic levitation system, eddy-current damping is utilized to suppress vibrations and improve dynamic response, particularly in high-precision applications such as micro-manipulation, space mechanisms, and energy harvesting devices (Jin et al., 2017). The integration of eddy-current damping with magnetic springs to create compact, oil-free, and reliable suspension systems eliminated the need for external power or complex controllers (Diez-Jimenez et al., 2021). Additionally, advancements in modeling and experimental validation have enabled precise control of damping characteristics by optimizing parameters such as conductor plate dimensions, material properties, and magnetic field configurations (Mehrtash and Khamesee, 2013). These developments highlight the versatility of eddy-current damping in addressing challenges related to vibration control and system stability, making it a promising solution for next-generation magnetic technologies (Elbuken et al., 2006).

In summary, to suppress the vibration induced by bolted-joint in the rotor-AMBs system based on eddy-current damping, the modelling of rotor-AMBs system considering eddy-current damping is essential and the influences of this damping on closed-loop system stability should be investigated.

2. Description of the system studied

The system is constituted with a steel shaft of 1.004 m length and 46 mm of diameter for a total weight of 10.35 kg (Fig. 1). It is supported by two identical AMBs powered in differential driving mode, with 8 poles and the action lines are positioned in the configuration load between axes. The bias current is 1.7 A and 0.25 mm for the air gap. Each AMB is supplied with a touch down bearings (TDBs) with 0.125 mm air gap, and two non-colocalized eddy current sensors. The AMBs are designed to generate a maximum dynamic force of 412 N. The exciter AMB located in the middle was not activated in this work and did not generate force. For the needs of this study, a bolted-joint aluminum disk (its size is fixed, thickness is 4 mm, radius is 45 mm, contact radius R_b is 7 mm) is assembled at the non-drive end and the bolted-joint torque M_b is adjusted in this work. Since the study is carried out only during levitation, the rotation is not taken account into this study.

A PID (proportional-integral-derivative) controller is designed to stabilize the rotor-AMBs system (sampling frequency is 10k Hz). An amplifier is used with 0.4 gain and 800 Hz cut- off frequency.

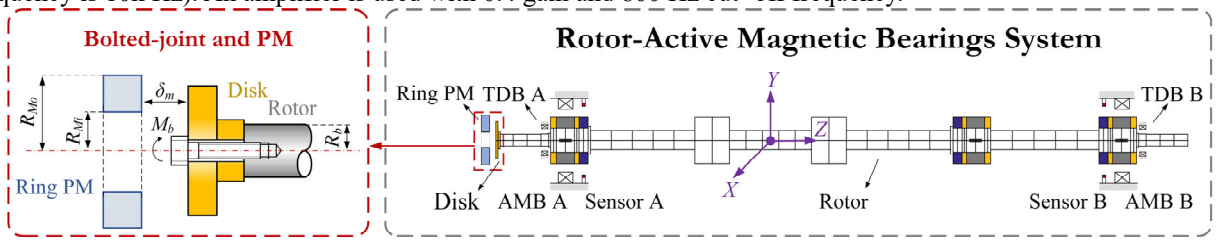

Fig. 1 Rotor-AMBs system with permanent magnet and bolted-joint disk.

In order to assess the influence of eddy-current damping on vibration suppression, the ring permanent magnet (PM) is arranged near the bolted-joint disk and axially aligned with the rotor (its size is fixed, thickness is 15 mm, outer radius R_{Mo} is 55 mm, inner radius R_{Mi} is 37.5 mm). The axial clearance δ_m between PM and disk is adjusted in this work.

3. Modelling of rotor-AMBs system considering bolted-joint assembly and eddy-current damping

The modelling approach of the eddy-current damping force will be presented first, then the rotor-AMBs system model considering bolted-joint assembly will be described.

3.1 Eddy-current damping force model

When the aluminum disk moves through a non-uniform electromagnetic field, a vortex electric field is induced within the material (Fig. 2). This field drives charge carriers to form closed-loop eddy currents due to the conductive continuity of the metal. According to Lenz's law, the induced currents generate opposing magnetic fields that resist the relative motion causing them. This resistance manifests as a damping force (Mehrtash and Khamesee, 2013).

In order to investigate the influence of eddy-current damping force on rotor AMBs system and optimize the structural parameter of permanent magnet, the analytical model of eddy-current damping is established based on Maxwell's equation and Faraday's law. There are some assumptions in the deduction of eddy-current damping force:

1) The high-frequency skin effect is ignored and the disk could be considered as a thin sheet where current density is assumed to be nearly uniform across the entire thickness of the conductor;
2) The PM material is homogeneous and rigidly magnetized;
3) Only the lateral vibration is considered, the axial and inclination vibrations of the disk are ignored.

Referring to Fig. 3, two coordinate systems are introduced to facilitate analysis: x, y, z Cartesian system fixed with respect to the immovable PM stator and x′, y′, z′ Cartesian system attached to the center of the disk.

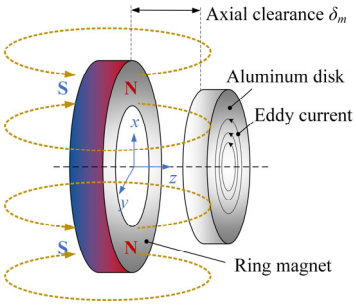

Fig. 2 Schematic of the generation of eddy current.

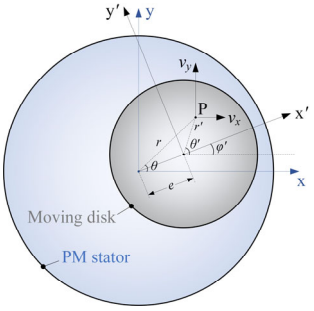

Fig. 3 Kinematic layout for the lateral vibration.

The eddy-current damping force is simplified as a linear force with respect to the velocity, ignoring the influence of high-frequency skin effect. The eddy-current damping force $\boldsymbol{F}_{ec}$ can be expressed as,

$$\boldsymbol{F}_{ec} = C_{ec} \cdot \left(-\boldsymbol{v}_d\right) \tag{1}$$

where C_{ec} is the eddy-current damping coefficient, $\boldsymbol{v}_d$ is the velocity vector of the disk. The C_{ec} is essential for the calculation of damping force. Firstly, the circumferential current density $K'_{\theta'}$ and radial current density $K'_{r'}$ should be determined. The governing equation can be expressed as,

$$\frac{1}{r'}\left[\frac{\partial\left(r' \cdot K'_{\theta'}\right)}{\partial r'} - \frac{\partial K'_{r'}}{\partial \theta'}\right] = -\sigma h \cdot v_r \frac{\partial B_z}{\partial r} \tag{2}$$

where σ is the electrical conductivity of the conductor, h is the thickness of the disk, v_r is the velocity of disk in the radial projection, B_z is the magnetic field strength (which is related to δ_m). Since eddy current is confined to the disk, the boundary condition could be written as Eq. (3) and R_d is the outer radius of the disk.

$$K'_{r'}\left(R_d, \theta'\right) = 0 \tag{3}$$

By solving Eq. (2) based on Eq. (3), the distributions of $K'_{\theta'}$ and $K'_{r'}$ are shown in Fig. 4.

By calculating the vector (K') of $K'_{\theta'}$ and $K'_{r'}$, the eddy-current coefficient C_{ec} can be obtained as,

$$C_{ec} = \iint_S K' \times B_z \mathrm{d}s = 0 \tag{4}$$

where s is the region of the disk.

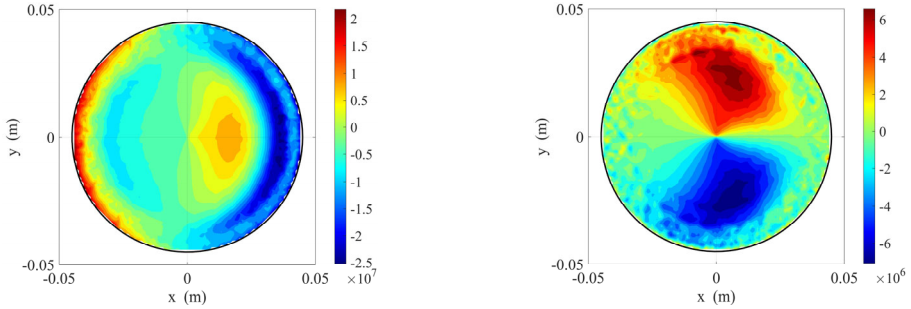

(a) Circumferential current density (A/m^2) (b) Radial current density (A/m^2)

Fig. 4 The values of current density (disk moves along the x direction).

To validate the accuracy of eddy-current damping, the eddy-current damping simulation is carried out based on the COMSOL software. The comparison of analytical results and COMSOL simulation results is shown in Fig. 5.

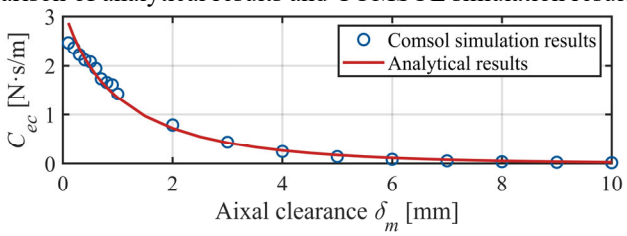

Fig. 5 The comparison of C_{ec} based on analytical model and COMSOL simulation model.

As shown in Fig. 5, the analytical results and COMSOL simulation results are in good agreement. Thus, the accuracy of the analytical eddy-current damping model is validated. And the C_{ec} increases exponentially as the decease of axial clearance δ_m.

3.2 Rotor-AMBs model considering bolted-joint assembly

The interface contact in the rotor is modelled as a uniformly distributed stiffness over the contact interface as shown in Fig. 6(a), where the disk and the rotor are joined together by bolted-joint assembly. The spring unit connects any point A on the rotor contact interface and its corresponding point B on the disk contact interface. The stiffness of the massless spring unit is referred to as contact stiffness, which can be subdivided into the normal contact stiffness k_{bn} and tangential contact stiffness k_{bt}.

The directions of k_{bn} and k_{bt} are perpendicular and parallel to the contact interface, respectively. The values of normal (tangential) contact stiffness k_{bn} (k_{bt}) under different torques and contact radii have been calculated based on the microscopic contact model and experimental identification in our previous research (Zhou et al., 2024).

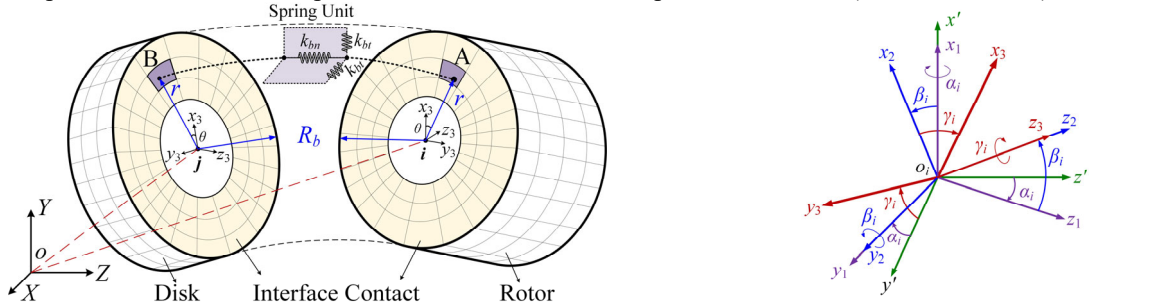

(a) Dynamic model of interface contact (b) Diagram of coordinate transformation

Fig. 6 Schematic diagram of the interface contact model formed by bolted-joint.

There is relative deformation between the contact interfaces when the rotor vibrates. The energy generated by the spring deformation is calculated to study the influence of interface contact. As shown in Fig. 6(b), floating coordinates o_i-$x_3y_3z_3$ and o_j-$x_3y_3z_3$ are established by taking the contact interface centers node i and node j as the coordinate origin

and coordinate transformation in order to obtain the relative deformations of the spring unit in X, Y, Z directions.

The total energy generated by the spring unit is obtained by summing up the unit spring energy Δu as Eq. (5).

$$\begin{aligned} U_b &= \iint_{\mathrm{H}} \frac{1}{2}\left(k_{bt}\cdot\Delta x^2 + k_{bt}\cdot\Delta y^2 + k_{bn}\cdot\Delta z^2\right)\mathrm{dH} \\ &= \frac{k_{bt}}{2}\iint_{\mathrm{H}}\mathrm{dH}\left[\Delta x_{ij}^{\ 2} + \Delta y_{ij}^{\ 2}\right] + \frac{k_{bn}}{2}\iint_{\mathrm{H}}\left[y^2\Delta\alpha_{ij}^{\ 2} + x^2\Delta\beta_{ij}^{\ 2}\right]\mathrm{dH} \end{aligned} \tag{5}$$

where $\Delta x=x_{\mathrm{B}}-x_{\mathrm{A}}$, $\Delta y=y_{\mathrm{B}}-y_{\mathrm{A}}$, $\Delta z=z_{\mathrm{B}}-z_{\mathrm{A}}$, H denotes the contact area of bolted-joint interface contact. The force vector $\boldsymbol{F}_{bc}$ generated by the interface can be obtained by calculating the partial derivative of the energy U_b with respect to the variable Δx_{ij} ($\Delta x_{ij}=x_i-x_j$), Δy_{ij} ($\Delta y_{ij}=y_i-y_j$), $\Delta\alpha_{ij}$ ($\Delta\alpha_{ij}=\alpha_i-\alpha_j$), $\Delta\beta_{ij}$ ($\Delta\beta_{ij}=\beta_i-\beta_j$).

$$\begin{aligned} \boldsymbol{F}_{bc} &= \begin{bmatrix} \partial U_b/\partial\Delta x_{ij} \\ \partial U_b/\partial\Delta y_{ij} \\ \partial U_b/\partial\Delta\alpha_{ij} \\ \partial U_b/\partial\Delta\beta_{ij} \end{bmatrix} = \begin{bmatrix} F_{bx} \\ F_{by} \\ F_{b\alpha} \\ F_{b\beta} \end{bmatrix} = \begin{bmatrix} k_{bt}\iint_{\mathrm{H}}\mathrm{dH}\cdot\Delta x_{ij} \\ k_{bt}\iint_{\mathrm{H}}\mathrm{dH}\cdot\Delta y_{ij} \\ k_{bn}\iint_{\mathrm{H}}y^2\mathrm{dH}\cdot\Delta\alpha_{ij} \\ k_{bn}\iint_{\mathrm{H}}x^2\mathrm{dH}\cdot\Delta\beta_{ij} \end{bmatrix} = \begin{bmatrix} Kb_x\left(\boldsymbol{q}_i,\boldsymbol{q}_j\right)\cdot\Delta x_{ij} \\ Kb_y\left(\boldsymbol{q}_i,\boldsymbol{q}_j\right)\cdot\Delta y_{ij} \\ Kb_\alpha\left(\boldsymbol{q}_i,\boldsymbol{q}_j\right)\cdot\Delta\alpha_{ij} \\ Kb_\beta\left(\boldsymbol{q}_i,\boldsymbol{q}_j\right)\cdot\Delta\beta_{ij} \end{bmatrix} \\ &= \mathrm{diag}\left[Kb_x \quad Kb_y \quad Kb_\alpha \quad Kb_\beta\right]\cdot\left[\mathrm{diag}(-1) \quad \mathrm{diag}(1)\right]\cdot\boldsymbol{T}_e\boldsymbol{q}_r = \boldsymbol{K}_b\boldsymbol{T}_e\boldsymbol{q}_r \end{aligned} \tag{6}$$

where the value of K_{sx}, K_{sy}, $K_{s\alpha}$, $K_{s\beta}$ are all related to $\boldsymbol{q}_i$ and $\boldsymbol{q}_j$, $\boldsymbol{T}_e$ is the transfer matrix of node i and j, $\boldsymbol{q}_r$ is the rotor displacement vector. The details about the bolted-joint rotor-AMBs model can be seen in the previous research [Zhou et al., 2024a].

The model of rotor-AMBs system considering interface contact consists of four parts as shown in Fig. 7: the contact stiffness model, the bolted-joint model, the rotor-AMBs model and the eddy-current damping force model. The effect of bolted-joint interface contact and eddy-current damping is modelled as the contact force $\boldsymbol{F}_{bc}$ and damping force $\boldsymbol{F}_{ec}$ acted on the rotor-AMBs model, respectively. The bolted-joint contact stiffness applied in bolted-joint model is calculated under different torque M_b and contact radius R_b based on the microscopic contact model, which has been established in the previous work together with the rotor-AMBs model.

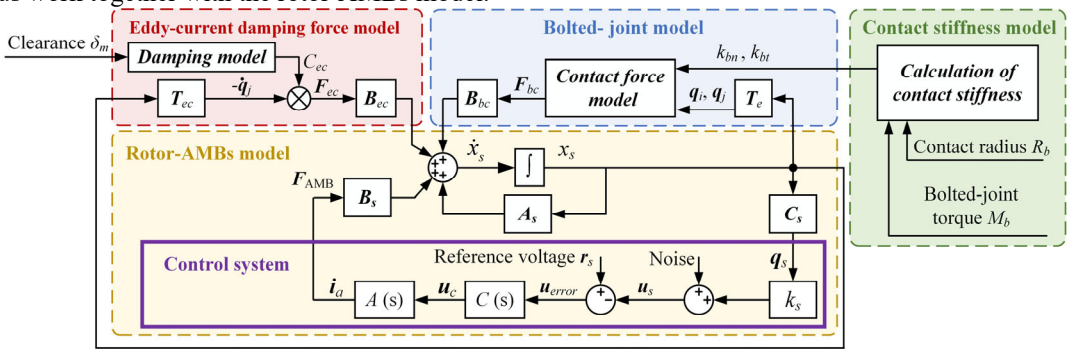

Fig. 7 Schematic of the rotor-AMBs system considering bolted-joint interface contact and eddy-current damping.

Finite element method is used. The shaft is modeled with 63 Bernoulli-Euler beam elements with two nodes and four degree of freedom (DOF) per node. Two radial translations and two associated rotations. The axial DOF is not considered in this study. The general equation of motion is obtained by applying Lagrange equation. Based on Eq. (1) and Eq. (6), the eddy-current force vector $\boldsymbol{F}_{ec}$ and contact force vector $\boldsymbol{F}_{bc}$ is then added.

$$\boldsymbol{M}_R\ddot{\boldsymbol{q}}_r + \boldsymbol{C}_R\dot{\boldsymbol{q}}_r + \boldsymbol{K}_R\boldsymbol{q}_r = \boldsymbol{T}_a^{\mathrm{T}}\boldsymbol{F}_{\mathrm{AMB}} + \boldsymbol{T}_{bc}^{\ \mathrm{T}}\boldsymbol{F}_{bc} + \boldsymbol{T}_{ec}^{\ \mathrm{T}}\boldsymbol{F}_{ec} = \boldsymbol{T}_a^{\mathrm{T}}\left(k_h\boldsymbol{T}_a\boldsymbol{q}_r + k_i\boldsymbol{i}_a\right) + \boldsymbol{T}_{bc}^{\ \mathrm{T}}\boldsymbol{F}_{bc} + \boldsymbol{T}_{ec}^{\ \mathrm{T}}\boldsymbol{C}_{ec}\boldsymbol{T}_{ec}\dot{\boldsymbol{q}}_r \tag{7}$$

where $\boldsymbol{M}_R$, $\boldsymbol{C}_R$ and $\boldsymbol{K}_R$ are the mass, damping and stiffness matrices of the system, respectively. The force vectors $\boldsymbol{F}_{\mathrm{AMB}}$ represents the electromagnetic force by the AMBs A and B in the X and Y directions, $\boldsymbol{T}_a$ is the transfer matrix of the AMB nodes, $\boldsymbol{T}_{bc}$ is the transfer matrix of node i, $\boldsymbol{T}_{ec}$ is the transfer matrix of node j. k_h (k_i) is the displacement (current) stiffness of the AMB. $\boldsymbol{i}_a$ is the control current of the AMB, which can be determined by,

$$\boldsymbol{i}_a = A(\mathrm{s})C(\mathrm{s})\left[\boldsymbol{r}_s - S(\mathrm{s})\boldsymbol{q}_s\right] = \frac{k_a(2\pi f_z)}{\mathrm{s}+2\pi f_z}\cdot\left(K_P + \frac{K_I}{\mathrm{s}} + \frac{K_D\mathrm{s}}{T_D\mathrm{s}+1}\right)\left(\boldsymbol{r}_s - k_s\boldsymbol{q}_s\right) \tag{8}$$

where $S(\mathrm{s})$, $A(\mathrm{s})$ and $C(\mathrm{s})$ are the transfer functions of the sensor, the amplifier and the controller, respectively, $\boldsymbol{q}_s$ is the displacement vector detected by sensors in the X and Y directions, k_s is the gain of sensor, k_a is the gain of power amplifier, f_z is the cut-off frequency, K_P, K_I and K_D respectively represent the proportional gain, the integral gain, the derivative gain, T_D is the derivative time constant to prevent magnifying the error signal by the controller in the high frequency ranges, and $\boldsymbol{r}_s$ is the reference voltage.

The state space model of the rotor-AMBs system considering the bolted-joint interface contact and eddy-current damping can be expressed as Eq. (9) by taking $\boldsymbol{x}_s = [\boldsymbol{q}_r \ \ \dot{\boldsymbol{q}}_r]^{\mathrm{T}}$.

$$\begin{cases} \dot{\boldsymbol{x}}_s = \boldsymbol{A}_s\boldsymbol{x}_s + \boldsymbol{B}_s\boldsymbol{i}_a + \boldsymbol{B}_{bc}\boldsymbol{F}_{bc} + \boldsymbol{B}_{ec}\boldsymbol{F}_{ec} \\ \boldsymbol{q}_s = \boldsymbol{C}_s\boldsymbol{x}_s \end{cases}$$
$$\boldsymbol{A}_s = \begin{bmatrix} 0_{256\times256} & I_{256\times256} \\ \boldsymbol{M}_R^{-1}\left(k_h\boldsymbol{T}_a^{\mathrm{T}}\boldsymbol{T}_a - \boldsymbol{K}_R\right) & -\boldsymbol{M}_R^{-1}\boldsymbol{C}_R \end{bmatrix}; \boldsymbol{B}_s = \begin{bmatrix} 0_{256\times4} \\ k_i\boldsymbol{M}_R^{-1}\boldsymbol{T}_a^{\mathrm{T}} \end{bmatrix}; \tag{9}$$
$$\boldsymbol{B}_{bc} = \begin{bmatrix} 0_{256\times4} \\ \boldsymbol{M}_R^{-1}\boldsymbol{T}_{bc}^{\mathrm{T}} \end{bmatrix}; \boldsymbol{B}_{ec} = \begin{bmatrix} 0_{256\times4} \\ \boldsymbol{M}_R^{-1}\boldsymbol{T}_{ec}^{\mathrm{T}} \end{bmatrix}; \boldsymbol{C}_s = \begin{bmatrix} \boldsymbol{T}_s & 0_{256\times4} \end{bmatrix}$$

where $\boldsymbol{x}_s$ is the state vector, $\boldsymbol{T}_s$ is the transfer matrix of the sensor nodes. $\boldsymbol{F}_{\mathrm{AMB}}$ is divided to negative stiffness part and control current part.

4. Results

Based on the rotor-AMBs model considering bolted-joint assembly and eddy-current damping, the dynamic analysis and stability analysis are carried out to investigate the influence of eddy-current damping on the vibration caused by bolted-joint assembly.

4.1 Dynamic analysis

Firstly, the free-free bending mode frequencies of the bolted-joint rotor (M_b = 3 N·m, R_b = 7 mm) are calculated based on the this model to identify which mode was affected by the bolted-joint assembly, and the results are given as: 1st bending mode frequency is 92.08 Hz, 2nd bending mode frequency is 257.81 Hz, 3rd bending mode frequency is 519.72 Hz, 4th bending mode frequency is 818.80 Hz, 5th bending mode frequency is 1081.28 Hz.

In previous study (Zhou et al., 2024), the influences of bolted-joint torque M_b and contact radius R_b on rotor responses and system stability have been investigated: when no bolted-joint applied, all roots of the system are stable, and that what is observed experimentally. On the other hand, when applying the bolted-joint, it can be noticed that the roots for the first two bending modes still stable for different values of M_b and R_b, but the roots for the 3rd, 4th and 5th modes move toward unstable locus as the increase of M_b and R_b. However, the amplitude of the 3rd and 5th mode is too small to influence the stability of the system, the instability of 4th bending mode is induced and the rotor vibrates at the 4th bending mode frequency. The increase of the bolted-joint torque and the contact radius will both increase the vibration amplitude.

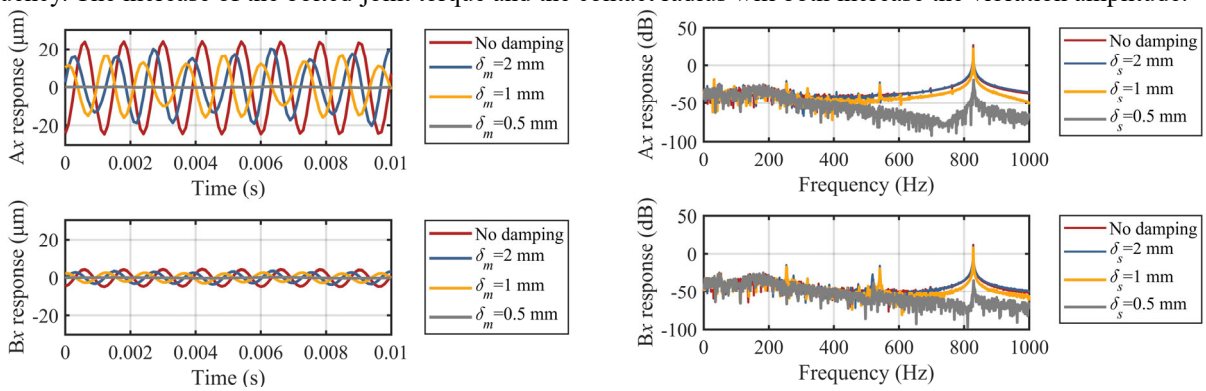

Fig. 8 Comparison of dynamic responses in simulation (different axial clearance).

In this study, appropriate control parameters should be tuned to ensure stable levitation of the rotor without interface contact and these parameters will be kept the same during different simulation phases to exclude the influence of the controller. The displacement responses in time and frequency domain in X direction for both AMBs under different axial clearance are presented in Fig. 8 for the value of M_b (3 N·m) and R_b (7 mm). The vibration amplitude of the 4th bending mode is dampened as the decrease of axial clearance δ_m (the increase of eddy-current damping coefficient C_{ec}).

4.2 Stability analysis and stable region

The root locus analysis is applied to study how the bolted-joint assembly and eddy-current damping force influence the stability of rotor-AMBs system. Based on Eq.(1) and Eq.(6), the eddy-current damping force can be expressed as $\boldsymbol{F}_{ec}=C_{ec}\cdot(-1)\cdot\boldsymbol{T}_{ec}\cdot\dot{\boldsymbol{q}}_r$, the contact force can be expressed as $\boldsymbol{F}_{bc}=\boldsymbol{K}_b\cdot\boldsymbol{T}_e\cdot\boldsymbol{q}_r$. The control current can be expressed as $\boldsymbol{i}_a=\boldsymbol{H}_s\cdot\boldsymbol{q}_s=\boldsymbol{H}_s\cdot\boldsymbol{T}_s\cdot\boldsymbol{q}_r$. Consequently, the state space in Eq. (9) can be transformed as.

$$\boldsymbol{A}_{sr}=\begin{bmatrix} 0_{256\times256} & I_{256\times256} \\ \boldsymbol{M}_R^{-1}\left(k_h\boldsymbol{T}_a^{\mathrm{T}}\boldsymbol{T}_a-\boldsymbol{K}_R+k_i\boldsymbol{T}_a^{\mathrm{T}}\boldsymbol{H}_s\boldsymbol{T}_s+\boldsymbol{T}_{bc}^{\mathrm{T}}\boldsymbol{K}_b\boldsymbol{T}_e\right) & -\boldsymbol{M}_R^{-1}\left(\boldsymbol{C}_R+\boldsymbol{T}_{ec}^{\mathrm{T}}C_{ec}\boldsymbol{T}_{ec}\right) \end{bmatrix} \tag{10}$$

The closed-loop system eigenvalues $\boldsymbol{\lambda}$ can be calculated as: det $(\boldsymbol{\lambda I}-\boldsymbol{A}_{sr})=0$.

As $\boldsymbol{A}_{sr}$ is dependent on the bolted-joint torque, the contact radius and the axial clearance, therefore, different eigenvalues will result for the different combination of the bolted-joint parameters and eddy current parameters.

In the situation that M_b is 3 N·m and R_b is 7 mm, decreasing the axial clearance δ_m from 3 mm to 0.1 mm, the root locus of the closed-loop system is shown in Fig. 9. As δ_m decreases, the characteristic roots of the first five bending modes move towards the negative direction of the real axis. To sum up, the decreasing of δ_m can increase the closed-loop stability of the 4th bending mode and have no unstable influence on other modes, which leads to vibration reduction of the 4th bending mode.

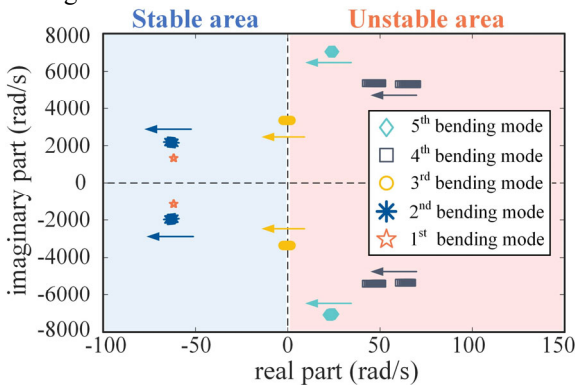

Fig. 9 Root locus of the closed-loop system for different axial clearances (0.1~3 mm).

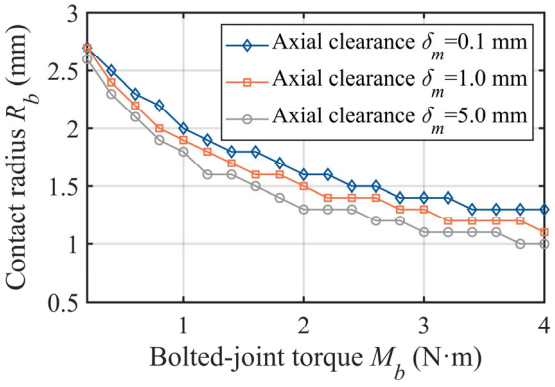

Fig. 10 Stable region as a function of bolted-joint parameters under different axial clearances.

Stemming from the root locus analysis, variables δ_m, M_b and R_b influence system stability. For further design optimization aiming at decreasing the influence of the bolted-joint interface contact, stable region (the region below the curves) can be obtained to guide the safe operation (Fig. 10). The stable parameter combinations of bolted-joint torque M_b and contact radius R_b under different axial clearance δ_m are specified based on the real parts of the 4th bending mode roots.

5. Conclusions

Numerical investigations are carried out to evaluate the effect of eddy-current damping on the stability of a bolted-joint rotor-AMBs system. The results obtained show that by decreasing the axial clearance between permanent magnet and the aluminum disk, the eddy-current damping is increased exponentially. The vibration amplitude in the 4th bending mode is suppressed due to the increase in eddy-current damping, which leads to the improvement of system stability. When the axial clearance is 0.5 mm, the vibration amplitude can be decrease by almost 99.5% in both directions. The unstable zones are identified as a function of the torque, contact radius and the axial clearance. The influencing parameters were pointed out, and their effects on the system dynamic behavior was studied. The stable parameter combinations are specified to guide the safe operation and this model will be used to conduct further investigations on the optimal design of the eddy-current damping. Experimental validation is undertaken and some of the results obtained could be presented

during the conference.

Acknowledgments and conflicts of interest

This work was supported by the National Natural Science Foundation of China (52475060).

The authors declare that they have no known competing financial interests or personal relationships that could have appeared to influence the work reported in this paper.

References

Schweitzer, G., Maslen, E., Magnetic bearings: theory, design, and application to rotating machinery, Berlin, Heidelberg: Springer Berlin Heidelberg (2009), pp. 1-17.

Diez-Jimenez, E., Alén-Cordero, C., Alcover-Sánchez, R. and Corral-Abad, E., Modelling and test of an integrated magnetic spring-eddy current damper for space applications, Actuators, Vol. 10, No. 1 (2021), p. 8.

Elbuken, C., Khamesee, M. B. and Yavuz, M., Eddy current damping for magnetic levitation: downscaling from macro- to micro-levitation, Journal of Physics D: Applied Physics, Vol. 39, No. 18 (2006), pp. 3932-3938.

Han, X., Zhou, J. and Zhou, Y., Analysis and suppression of self-excited vibration of flexible rotor AMBs system, Journal of Vibration Engineering & Technologies, Vol. 9, No. 8 (2021), pp. 1911-1922.

Jin, L., Zheng, J., Li, H., Li, J., Zhou, Z., Zhang, Y. and Deng, Z., Effect of eddy current damper on the dynamic vibration characteristics of high-temperature superconducting maglev system, IEEE Transactions on Applied Superconductivity, Vol. 27, No. 3 (2017), pp. 1-6.

Mehrtash, M. and Khamesee, M. B., Modeling and analysis of eddy-current damping effect in horizontal motions for a high-precision magnetic navigation platform, IEEE Transactions on Magnetics, Vol. 49, No. 8 (2013), pp. 4801-4810.

Park, I-S., Sohn, C. H. and Kim, H. J., Acoustic damping enhanced by gaps in baffled injectors in an acoustic chamber, Journal of Sound and Vibration, Vol. 330, No. 12 (2011), pp. 2747-2757.

Wei, S., Zhou, J., Han, X. and Zheng, S., A simplified analysis method and suppression of the modalities of a magnetic levitation turbo rotor system, Vacuum, Vol. 217 (2023), p. 112452.

Zeng, K., Zhou, Y., Xu, Y. and Zhou, J., Modal vibration suppression for magnetically levitated rotor considering significant gyroscopic effects and interface contact, Actuators, Vol. 14, No. 2 (2025), p. 76.

Zhou, Y., Zhou, J., Mahfoud, J., Zhang, Y. and Xu, Y., Modelling and validation of rotor-active magnetic bearing system considering interface contact, in Proceedings of the 11th IFToMM International Conference on Rotordynamics, Cham: Springer International Publishing (2023), pp. 374-390.

Zhou, Y., Zhou, J., Wang, Y., Zhang, Y., Xu, Y. and Lin, Z., Investigations on the modal vibration caused by bolted joint interface contact in the rotor-AMBs systems: Modelling and experimentation, Applied Mathematical Modelling, Vol. 134 (2024a), pp. 249-267.

Zhou, Y., Zhou, J., Wang, Y., Zhang, Y. and Xu, Y., Optimal phase compensation for a rotor-AMB system considering interface contact, Journal of Vibration and Control, Vol. 30, No. 9-10 (2024b), pp. 2059-2071.

Zhu, W., Zhao, Z., Zhou, X., Cao, X., Ye, M., Cao, C. and Alam, M. M., Research on damping hole optimization of hydro-pneumatic suspension for mining trucks under variable load conditions, Actuators, Vol. 13, No. 5 (2024), p. 163.